Molecular Physics
Vol. 108, No. 11, 10 June 2010, 1471–1479

Taylor & Francis
Taylor & Francis Group

RESEARCH ARTICLE

Nonadiabatic dynamics by mean-field and surface-hopping approaches: energy conservation considerations

Steven L. Fiedler[a]* and Jussi Eloranta[b]

[a]*Department of Mechanical Engineering, The University of Michigan, 2250 G.G. Brown, 2350 Hayward St., Ann Arbor, Michigan 48109-2125, USA;* [b]*Department of Chemistry and Biochemistry, California State University at Northridge, 18111 Nordhoff St., Northridge, California 91330-8262, USA*

(*Received 14 November 2009; final version received 17 February 2010*)

The mean-field and surface-hopping approaches are mixed quantum-classical algorithms designed to efficiently incorporate nonadiabatic effects into molecular dynamics simulations. In this report, analytical relations underpinning the two methods are derived within the adiabatic basis to provide an implementation-level overview, with particular attention given to two avoidable sources of energy conservation deviation. It is not widely known that accuracy improvements can be obtained at negligible computational expense by allowing: (a) construction of the Schrödinger equation to account for analytic electronic phase propagation, and (b) inclusion of a Hellman–Feynman correctional term in the calculation of atomic forces. Particular emphasis on the algebraic formalism contrasts these inherent approximations, *vis-à-vis* the correctional approaches. The sensitivity of energy conservation with respect to phase propagation is exemplified by simulation of Xe_3^+ molecular photodissociation on the repulsive $\Pi(1/2)_u$ excited surface. Simulations of a representative two-state avoided crossing system are presented to exemplify analytic quantities of the mean-field and surface-hopping approaches as well as to illustrate the inclusion of the Hellman–Feynman correctional term. Nonadiabatic propagation of the molecular wavefunction is observed by monitoring ground and excited state occupational probabilities, energy conservation, and nonadiabatic coupling as the system evolves along the model potential energy surfaces.

Keywords: computer simulation; nonadiabatic dynamics; mean-field; surface-hopping; conical intersection; Born–Oppenheimer

1. Introduction

Nonadiabatic transitions are a quantum mechanical effect that can affect molecular behaviour in 'ultrafast' conditions, e.g. following excitation or molecular collisions. Spontaneous non-radiative electronic transitions may occur based on correlated dynamics of electrons to that of the nuclei. Accordingly, atomic motions do not necessarily follow a single (adiabatic) potential energy hypersurface as designated by the Born–Oppenheimer approximation. Known processes that may proceed through nonadiabatic transitions include photodissociation [1], surface femtochemistry [2] and scattering measurements [3], photosynthetic processes [4,5], tautomerisation of nucleic bases [6], and protein transfer in enzyme reactions [7]. Computer simulations based on Molecular Dynamics (MD), where inter- and intra-molecular forces are calculated on the fly and atomic positions are subsequently propagated by application of Newton's integrated equations of motion [8], are amenable to incorporating the physics of these effects. To this end, mixed quantum-classical approaches have been developed to treat these systems in a computationally tractable manner, including the ubiquitous mean-field and surface-hopping methods [9]. Accurately described by their respective names, the mean-field approach, based on the Ehrenfest theorem [10], specifies atomic forces to be obtained from an 'averaged' potential, and the surface-hopping approach evolves atomic dynamics on a single surface with a probabilistic evaluation of a surface 'hopping' event at every time step. While neither method can completely depict the quantum nature of the system, it has been shown that their applicability and limitations are understood [3]. A benchmark of accurate molecular simulation is energy conservation. In this article, two unintended sources of energy conservation loss are discussed in the implementation of the mean-field and

*Corresponding author. Email: fiedler@umich.edu

ISSN 0026–8976 print/ISSN 1362–3028 online

DOI: 10.1080/00268971003720314
http://www.informaworld.com

surface-hopping approaches. In this context, we seek to expand upon several excellent reviews [3,11–14] and provide derivation of fundamental relations upon which these two practical implementations are based. Subsequent derivation of dependent quantities are carried through, to provide a comprehensive reference for implementation.

2. Electronic equations of motion

For both the mean-field and surface-hopping methods, the electronic wave function is composed as a superposition of adiabatic states, $|\phi_0\rangle, |\phi_1\rangle, \ldots$

$$|\psi(t)\rangle = a_0(t)\exp\left(-\mathrm{i}/\hbar\int_0^t E_0(\tau)\mathrm{d}\tau\right)|\phi_0(t)\rangle + a_1(t)\exp\left(-\mathrm{i}/\hbar\int_0^t E_1(\tau)\mathrm{d}\tau\right)|\phi_1(t)\rangle + \cdots, \quad (1)$$

with conservation of the norm of the expansion coefficients: $a_0^2(t) + a_1^2(t) + \cdots = 1$. To simplify the algebra, the phase is commonly included with the expansion coefficient:

$$|\psi(t)\rangle = b_0(t)|\phi_0\rangle + b_1(t)|\phi_1\rangle + \cdots, \quad (2)$$

where

$$b_j(t) = a_j(t)\exp\left(-\mathrm{i}/\hbar\int_0^t E_j(\tau)\mathrm{d}\tau\right). \quad (3)$$

This simplified approach introduces energy conservation inaccuracies when numerical propagation of phases is used (Figure 1). This is due to the fact that while the phase term in (1) can be analytically evaluated, the 'bundled' phase in (2) is implicitly propagated numerically. To simulate the evolution of a system, the time-dependent Schrödinger equation,

$$\left|\frac{\partial\psi(t)}{\partial t}\right\rangle = -\frac{\mathrm{i}}{\hbar}\hat{\mathbf{H}}|\psi(t)\rangle, \quad (4)$$

allows temporal derivation of the expansion coefficient values, $\{\mathrm{d}a_i(t)/\mathrm{d}t\}$ or $\{\mathrm{d}b_i(t)/\mathrm{d}t\}$, in terms of extractable values from the simulation (Sections 2.1 and 2.2 respectively). The propagated values can then be determined by application of standard numerical integration techniques [16].

2.1. *Differential form of expansion coefficients*

Limiting the electronic wavefunction in (1) to two states for simplicity, the temporal differential can be equated to familiar quantites by substitution into (4),

$$\begin{aligned}
&\frac{\mathrm{d}a_0(t)}{\mathrm{d}t}\exp\left(-\frac{\mathrm{i}}{\hbar}\int_0^t E_0(\tau)\mathrm{d}\tau\right)|\phi_0\rangle \\
&\quad - \frac{a_0(t)\mathrm{i}E_0(t)}{\hbar}\exp\left(-\frac{\mathrm{i}}{\hbar}\int_0^t E_0(\tau)\mathrm{d}\tau\right)|\phi_0\rangle \\
&\quad + a_0(t)\exp\left(-\frac{\mathrm{i}}{\hbar}\int_0^t E_0(\tau)\mathrm{d}\tau\right)\left|\frac{\partial\phi_0}{\partial t}\right\rangle \\
&\quad + \frac{\mathrm{d}a_1(t)}{\mathrm{d}t}\exp\left(-\frac{\mathrm{i}}{\hbar}\int_0^t E_1(\tau)\mathrm{d}\tau\right)|\phi_1\rangle \\
&\quad - \frac{a_1(t)\mathrm{i}E_1(t)}{\hbar}\exp\left(-\frac{\mathrm{i}}{\hbar}\int_0^t E_1(\tau)\mathrm{d}\tau\right)|\phi_1\rangle \\
&\quad + a_1(t)\exp\left(-\frac{\mathrm{i}}{\hbar}\int_0^t E_1(\tau)\mathrm{d}\tau\right)\left|\frac{\partial\phi_1}{\partial t}\right\rangle \\
&= -\frac{\mathrm{i}E_0(t)}{\hbar}a_0(t)\exp\left(-\frac{\mathrm{i}}{\hbar}\int_0^t E_0(\tau)\mathrm{d}\tau\right)|\phi_0\rangle \\
&\quad - \frac{\mathrm{i}E_1(t)}{\hbar}a_1(t)\exp\left(-\frac{\mathrm{i}}{\hbar}\int_0^t E_1(\tau)\mathrm{d}\tau\right)|\phi_1\rangle. \quad (5)
\end{aligned}$$

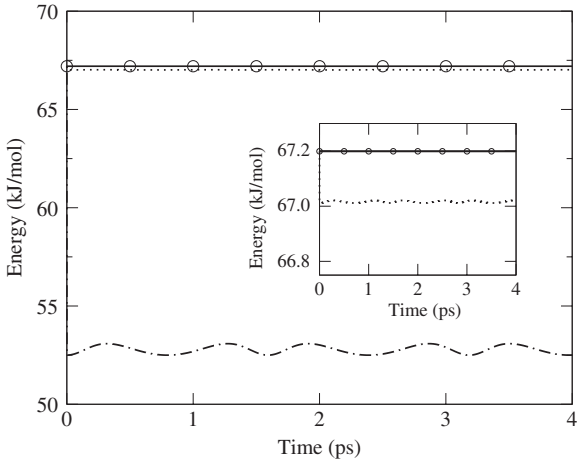

Figure 1. Total energy conservation of the linear, symmetric Xe_3^+ dissociation on the $\Pi(1/2)_u$ excited state, contrasting analytical and numerical phase propagation (magnified in inset). Trajectories based on analytical phase evaluation (Section 2.1) can be seen to preserve energy conservation relatively well on transitioning from small to larger time steps as compared to numerical phase propagation (Section 2.2): analytical 0.1 fs time step (circle), analytical 1 fs time step (solid line), numerical 0.1 fs time step (dotted line), and numerical 1 fs time step (dashed line). Simulations employed the mean-field approach with both analytical and numerical expansion coefficients integrated by Crank–Nicolson method. The initial Xe_3^+ nearest neighbor atoms were separated by 0.4 nm and remaining simulation parameters are specified in [15]. The initial energy drop in the numerical phase propagation calculations is attributed to an artifact of the Crank–Nicolson method.

Multiplying (5) from the left by $\langle\boldsymbol{\phi}_0|$ and integrating yields,

$$\frac{\mathrm{d}a_0(t)}{\mathrm{d}t}\exp\left(-\frac{\mathrm{i}}{\hbar}\int_0^t E_0(\tau)\mathrm{d}\tau\right) + a_1(t)\exp\left(-\frac{\mathrm{i}}{\hbar}\int_0^t E_1(\tau)\mathrm{d}\tau\right)\left\langle\boldsymbol{\phi}_0\left|\frac{\partial\boldsymbol{\phi}_1}{\partial t}\right\rangle\right. = 0. \quad (6)$$

Note that $|\boldsymbol{\phi}_0\rangle$ and $|\boldsymbol{\phi}_1\rangle$ are orthonormal. Provided $|\boldsymbol{\phi}_i\rangle$ is real, e.g. neglecting spin–orbit coupling, $\langle\boldsymbol{\phi}_i|\partial\boldsymbol{\phi}_i/\partial t\rangle = 0$ (Appendix 1). Rearranging (6),

$$\frac{\mathrm{d}a_0(t)}{\mathrm{d}t} = -a_1(t)\left\langle\boldsymbol{\phi}_0\left|\frac{\partial\boldsymbol{\phi}_1}{\partial t}\right\rangle\right.\exp\left(-\frac{\mathrm{i}}{\hbar}\int_0^t E_1(\tau) - E_0(\tau)\mathrm{d}\tau\right), \quad (7)$$

or more generally for more than two levels,

$$\frac{\mathrm{d}a_j(t)}{\mathrm{d}t} = \sum_{k\neq j} -a_k(t)\left\langle\boldsymbol{\phi}_j\left|\frac{\partial\boldsymbol{\phi}_k}{\partial t}\right\rangle\right.\exp\left(-\frac{\mathrm{i}}{\hbar}\int_0^t E_k(\tau) - E_j(\tau)\mathrm{d}\tau\right). \quad (8)$$

For implementation, the integral in (7) can be written as a summation over finite time steps. Additionally, it is advantageous to keep a running total of the eigenvalues, E_j, which can be applied in the numerical evaluation of the exponential.

2.2. *Differential form of consolidated expansion coefficients and phase*

For the two state system, to determine $\mathrm{d}b_0(t)/\mathrm{d}t$ and $\mathrm{d}b_1(t)/\mathrm{d}t$ we substitute (2) into the Schrödinger equation, (4):

$$\frac{\mathrm{d}b_0(t)}{\mathrm{d}t}|\boldsymbol{\phi}_0\rangle + b_0(t)\left|\frac{\partial\boldsymbol{\phi}_0}{\partial t}\right\rangle + \frac{\mathrm{d}b_1(t)}{\mathrm{d}t}|\boldsymbol{\phi}_1\rangle + b_1(t)\left|\frac{\partial\boldsymbol{\phi}_1}{\partial t}\right\rangle = -\frac{\mathrm{i}}{\hbar}E_0(t)b_0(t)|\boldsymbol{\phi}_0\rangle - \frac{\mathrm{i}}{\hbar}E_1(t)b_1(t)|\boldsymbol{\phi}_1\rangle. \quad (9)$$

To remove the presence of the eigenstate basis functions in (9), multiply from the left by $\langle\boldsymbol{\phi}_0|$ and integrate. As introduced in Section 2.1, $\langle\boldsymbol{\phi}_0\,|\,\boldsymbol{\phi}_0\rangle = 1$ and $\langle\boldsymbol{\phi}_0\,|\,\boldsymbol{\phi}_1\rangle = 0$ and $\langle\boldsymbol{\phi}_0\,|\,\partial\boldsymbol{\phi}_0/\partial t\rangle = 0$. Thus

$$\frac{\mathrm{d}b_0(t)}{\mathrm{d}t} = -\frac{\mathrm{i}}{\hbar}E_0(t)b_0(t) - b_1(t)\langle\boldsymbol{\phi}_0\left|\frac{\partial\boldsymbol{\phi}_1}{\partial t}\right\rangle, \quad (10)$$

and expanded for more than two levels,

$$\frac{\mathrm{d}b_j(t)}{\mathrm{d}t} = -\frac{\mathrm{i}}{\hbar}E_j(t)b_j(t) - \sum_{k\neq j} b_k(t)\langle\boldsymbol{\phi}_j\left|\frac{\partial\boldsymbol{\phi}_k}{\partial t}\right\rangle. \quad (11)$$

2.3. *Determination of the nonadiabatic coupling term:* $\langle\boldsymbol{\phi}_j\,|\,\partial\boldsymbol{\phi}_k/\partial t\rangle$

The quantities $\langle\boldsymbol{\phi}_j\,|\,\partial\boldsymbol{\phi}_k/\partial t\rangle$ in (7) and (10) are defined as the coupling term d_{jk}. By the chain rule, d_{jk} can be expanded in terms of q_m nuclear degrees of freedom:

$$d_{jk} = \left\langle\boldsymbol{\phi}_j\left|\frac{\partial\boldsymbol{\phi}_k}{\partial t}\right\rangle\right. = \left\langle\boldsymbol{\phi}_j\left|\sum_{m=1}^{3N}\frac{\partial\boldsymbol{\phi}_k}{\partial q_m}\times\frac{\mathrm{d}q_m}{\mathrm{d}t}\right\rangle\right., \quad (12)$$

where N is the number of nuclei. The velocity of a particular degree of freedom ($\mathrm{d}q_m/\mathrm{d}t$) can be removed from the integral on the right side, as it is constant with respect to integration over the electronic coordinates. Thus,

$$\left\langle\boldsymbol{\phi}_j\left|\frac{\partial\boldsymbol{\phi}_k}{\partial t}\right\rangle\right. = \sum_m\langle\boldsymbol{\phi}_j|\frac{\partial}{\partial q_m}|\boldsymbol{\phi}_k\rangle\times\frac{\mathrm{d}q_m}{\mathrm{d}t}, \quad (13)$$

or more succinctly,

$$d_{jk} = \boldsymbol{D}_{jk}\cdot\frac{\mathrm{d}\boldsymbol{q}}{\mathrm{d}t}, \quad (14)$$

where $\boldsymbol{D}_{jk}$ denotes the nonadiabatic coupling vector $\{D_{jk,m}\}$, and $\mathrm{d}\boldsymbol{q}/\mathrm{d}t$ as the nuclear velocity vector. To solve for $\boldsymbol{D}_{jk}$, differentiate the time-independent Schrödinger equation with respect to nuclear coordinate, q_m,

$$\frac{\partial}{\partial q_m}\left[\hat{\mathbf{H}}(q_m,t)|\boldsymbol{\phi}_k(q_m,t)\rangle\right] = \frac{\partial}{\partial q_m}\left[E_k|\boldsymbol{\phi}_k(q_m,t)\rangle\right], \quad (15)$$

$$\frac{\partial\hat{\mathbf{H}}(q_m)}{\partial q_m}|\boldsymbol{\phi}_k\rangle + \hat{\mathbf{H}}(q_m)\left|\frac{\partial\boldsymbol{\phi}_k}{\partial q_m}\right\rangle = \frac{\partial E_k}{\partial q_m}|\boldsymbol{\phi}_k\rangle + E_k\left|\frac{\partial\boldsymbol{\phi}_k}{\partial q_m}\right\rangle. \quad (16)$$

Multiplying (16) from the left by $\langle\boldsymbol{\phi}_j\,|$ and integrating yields,

$$\langle\boldsymbol{\phi}_j|\frac{\partial\hat{\mathbf{H}}}{\partial q_m}|\boldsymbol{\phi}_k\rangle + E_j\left\langle\boldsymbol{\phi}_j\left|\frac{\partial\boldsymbol{\phi}_k}{\partial q_m}\right\rangle\right. = E_k\left\langle\boldsymbol{\phi}_j\left|\frac{\partial\boldsymbol{\phi}_k}{\partial q_m}\right\rangle\right., \quad (17)$$

$$\langle\boldsymbol{\phi}_j|\frac{\partial\hat{\mathbf{H}}}{\partial q_m}|\boldsymbol{\phi}_k\rangle = (E_k - E_j)\left\langle\boldsymbol{\phi}_j\left|\frac{\partial\boldsymbol{\phi}_k}{\partial q_m}\right\rangle\right., \quad (18)$$

$$D_{jk,m} = \left\langle\boldsymbol{\phi}_j\left|\frac{\partial\boldsymbol{\phi}_k}{\partial q_m}\right\rangle\right. = \frac{\langle\boldsymbol{\phi}_j|\,(\partial\hat{\mathbf{H}}/\partial\mathbf{q_m})|\boldsymbol{\phi}_\mathbf{k}\rangle}{(E_k - E_j)}. \quad (19)$$

Finally,

$$d_{jk} = \left\langle\boldsymbol{\phi}_j\left|\frac{\partial\boldsymbol{\phi}_k}{\mathrm{d}t}\right\rangle\right. = \sum_m D_{jk,m}\times\frac{\mathrm{d}q_m}{\mathrm{d}t} = \sum_m\frac{\langle\boldsymbol{\phi}_j|\,(\partial\hat{\mathbf{H}}/\partial\mathbf{q_m})|\boldsymbol{\phi}_\mathbf{k}\rangle}{(E_k - E_j)}\times\frac{\mathrm{d}q_m}{\mathrm{d}t}. \quad (20)$$

2.4. *Implementation*

The propagation of the analytical wavefunction defined by (1) can be easily demonstrated by integrating the corresponding differential form of the $\{a_i\}$ expansion coefficients, defined by (8), with the Euler method. At time, $t = t + \mathrm{d}t$, $\psi(t)$ evolves to:

$$\begin{aligned}&\left|\boldsymbol{\psi}(t+\mathrm{d}t)\right\rangle \\ &= a_0(t+\mathrm{d}t)\exp\left(-\mathrm{i}/\hbar\int_0^{t+\mathrm{d}t}E_0(\tau)\mathrm{d}\tau\right)\left|\boldsymbol{\phi}_0(t+\mathrm{d}t)\right\rangle \\ &\quad + a_1(t+\mathrm{d}t)\exp\left(-\mathrm{i}/\hbar\int_0^{t+\mathrm{d}t}E_1(\tau)\mathrm{d}\tau\right) \\ &\quad \times\left|\boldsymbol{\phi}_1(t+\mathrm{d}t)\right\rangle+\cdots. \end{aligned} \tag{21}$$

To first approximation, the expansion coefficients can be defined in terms of expansion coefficient values at time, t, by a Taylor expansion,

$$a_i(t+\mathrm{d}t) = a_i(t) + \frac{\mathrm{d}a_i(t)}{\mathrm{d}t}\,\mathrm{d}t. \tag{22}$$

Substituting (8) and (20) into (22) yields

$$\begin{aligned}&a_j(t+\mathrm{d}t) \\ &= a_j(t) - \mathrm{d}t\sum_{k\neq j}a_k(t)\left(\sum_m\frac{\langle\boldsymbol{\phi}_j|\,(\partial\hat{\mathbf{H}}/\partial\mathbf{q_m})|\boldsymbol{\phi}_\mathbf{k}\rangle}{(E_k-E_j)}\times\frac{\mathrm{d}q_m}{\mathrm{d}t}\right) \\ &\quad\times\exp\left(-\frac{\mathrm{i}}{\hbar}\int_0^t E_k(\tau)-E_j(\tau)\mathrm{d}\tau\right). \end{aligned} \tag{23}$$

In this case, the propagation of the nuclear wavefunctions precedes that of the electronic, and the adiabatic basis functions, $|\phi_j(t+\mathrm{d}t)\rangle$ are obtained as eigenfunctions of the diagonalised Hamiltonian. The electronic wavefunction can also be expressed in terms of a diabatic basis set [12], which may be preferable in curve crossing (conical intersection) regions, where the adiabatic basis functions vary rapidly with respect to small changes in the nuclear coordinates.

3. Mean field

3.1. *Mean-field potential energy*

Using the two-level wave function from (1), the Schrödinger equation for energy can be solved,

$$\begin{aligned}E &= \langle\boldsymbol{\psi}|\hat{\mathbf{H}}|\boldsymbol{\psi}\rangle \\ &= \left\langle a_0(t)\exp\left(-\frac{\mathrm{i}}{\hbar}\int_0^t E_0(\tau)\,\mathrm{d}\tau\right)\boldsymbol{\phi}_0|\hat{\mathbf{H}}|a_0(t)\right. \\ &\quad\left.\times\exp\left(-\frac{\mathrm{i}}{\hbar}\int_0^t E_0(\tau)\,\mathrm{d}\tau\right)\boldsymbol{\phi}_0\right\rangle \\ &\quad+\left\langle a_1(t)\exp\left(-\frac{\mathrm{i}}{\hbar}\int_0^t E_1(\tau)\,\mathrm{d}\tau\right)\boldsymbol{\phi}_1|\hat{\mathbf{H}}|a_1(t)\right. \\ &\quad\left.\times\exp\left(-\frac{\mathrm{i}}{\hbar}\int_0^t E_1(\tau)\,\mathrm{d}\tau\right)\boldsymbol{\phi}_1\right\rangle. \end{aligned} \tag{24}$$

We can remove a_0, a_1, and the phase terms from the integrals since they are not dependent on the electronic coordinate:

$$E = a_0(t)^*a_0(t)\langle\boldsymbol{\phi}_0|\hat{\mathbf{H}}|\boldsymbol{\phi}_0\rangle + a_1(t)^*a_1(t)\langle\boldsymbol{\phi}_1|\hat{\mathbf{H}}|\boldsymbol{\phi}_1\rangle. \tag{25}$$

To monitor energy conservation, it is necessary to explicitly calculate the total potential energy. For consideration of multiple electronic states, (25) can be reduced to:

$$E = \sum_j a_j^*(t)a_j(t)E_j. \tag{26}$$

3.2. *Mean-field forces*

Taking the gradient of energy in (25) with respect to the q_m degree of freedom yields

$$\begin{aligned}\frac{\partial E}{\partial q_m} &= \frac{\mathrm{d}a_0(t)^*}{\mathrm{d}q_m}a_0(t)E_0 + a_0(t)^*\frac{\mathrm{d}a_0(t)}{\mathrm{d}q_m}E_0 \\ &\quad + a_0(t)^*a_0(t)E_0\left\langle\frac{\partial\boldsymbol{\phi}_0}{\partial q_m}\middle|\boldsymbol{\phi}_0\right\rangle + a_0(t)^*a_0(t)\langle\boldsymbol{\phi}_0|\frac{\partial\hat{\mathbf{H}}}{\partial q_m}|\boldsymbol{\phi}_0\rangle \\ &\quad + a_0(t)^*a_0(t)E_0\left\langle\boldsymbol{\phi}_0\middle|\frac{\partial\boldsymbol{\phi}_0}{\partial q_m}\right\rangle+\cdots, \end{aligned} \tag{27}$$

for the first term in (25). Rearranging (27) yields

$$\begin{aligned}\frac{\partial E}{\partial q_m} &= a_0(t)^*a_0(t)\langle\boldsymbol{\phi}_0|\frac{\partial\hat{\mathbf{H}}}{\partial q_m}|\boldsymbol{\phi}_0\rangle \\ &\quad + E_0\left(\frac{\mathrm{d}a_0^*(t)}{\mathrm{d}q_m}a_0(t) + a_0(t)^*\frac{\mathrm{d}a_0(t)}{\mathrm{d}q_m}\right) \\ &\quad + a_0(t)^*a_0(t)E_0\left(\left\langle\frac{\partial\boldsymbol{\phi}_0}{\partial q_m}\middle|\boldsymbol{\phi}_0\right\rangle + \left\langle\boldsymbol{\phi}_0\middle|\frac{\partial\boldsymbol{\phi}_0}{\partial q_m}\right\rangle\right)+\cdots. \end{aligned} \tag{28}$$

The last printed term on the right of (28) is zero:

$$\begin{gathered}\langle\boldsymbol{\phi}_0|\boldsymbol{\phi}_0\rangle = 1, \quad \frac{\partial}{\partial q_m}\langle\boldsymbol{\phi}_0|\boldsymbol{\phi}_0\rangle = 0, \\ \left\langle\frac{\partial\boldsymbol{\phi}_0}{\partial q_m}\middle|\boldsymbol{\phi}_0\right\rangle + \left\langle\boldsymbol{\phi}_0\middle|\frac{\partial\boldsymbol{\phi}_0}{\partial q_m}\right\rangle = 0. \end{gathered} \tag{29}$$

From (28) the total force on the degree of freedom q_m is:

$$F_{q_m} = -\frac{\partial E}{\partial q_m} = -\sum_j a_j^*(t)a_j(t)\langle\boldsymbol{\phi}_j|\frac{\partial\hat{\mathbf{H}}}{\partial q_m}|\boldsymbol{\phi}_j\rangle + E_j\left(\frac{\mathrm{d}a_j^*(t)}{\mathrm{d}q_m}a_j + a_j^*(t)\frac{\mathrm{d}a_j(t)}{\mathrm{d}q_m}\right). \quad (30)$$

Note (30) differs from the conventional appearance of the Hellmann–Feynman theorem by the presence of the second term on the right [12]. The theorem is dependent though on the condition that $|\boldsymbol{\phi}\rangle$ is an eigenstate of the Hamiltonian. Normally this second term is small, however, it should be included for accurate accounting of energy conservation. Finally using the chain rule, (30) can be expressed in more familiar quantities:

$$F_{q_m} = -\frac{\partial E}{\partial q_m} = -\sum_j a_j^*(t)a_j(t)\langle\boldsymbol{\phi}_j|\frac{\partial\hat{\mathbf{H}}}{\partial q_m}|\boldsymbol{\phi}_j\rangle + E_j \times \frac{\mathrm{d}t}{\mathrm{d}q_m}\left(\frac{\mathrm{d}a_j^*(t)}{\mathrm{d}t}a_j(t) + a_j^*(t)\frac{\mathrm{d}a_j(t)}{\mathrm{d}t}\right), \quad (31)$$

where j sums over the states. For implementation purposes, $\mathrm{d}q_m/\mathrm{d}t$ is equivalent to the atomic velocity, v_m (along the mth coordinate). Thus (31) can be written as:

$$F_{q_m} = -\frac{\partial E}{\partial q_m} = -\sum_j a_j(t)^* a_j(t)\langle\boldsymbol{\phi}_j|\frac{\partial\hat{\mathbf{H}}}{\partial q_m}|\boldsymbol{\phi}_j\rangle + \frac{E_j}{v_m}\left(\frac{\mathrm{d}a_j^*(t)}{\mathrm{d}t}a_j(t) + a_j^*(t)\frac{\mathrm{d}a_j(t)}{\mathrm{d}t}\right). \quad (32)$$

4. Surface-hopping

4.1. *Hopping probability*

The expansion coefficients $a_j(t)$ in (1) or $b_j(t)$ in (3) can be described in density matrix notation, with ρ_{jj} as the population in state j and ρ_{jk} as the coherence between the states j and k.

$$\rho_{jj} = a_j^*(t)a_j(t), \quad (33)$$

$$\rho_{jk} = a_j^*(t)a_k(t). \quad (34)$$

The hopping probability between states j and k is then directly equated to the portion of occupational probability transferred from state j to state k over $\mathrm{d}t$. The quantity or change of occupational probability of state j within time Δt is:

$$\Delta\rho_{jj}(t) = \dot{\rho}_{jj}(t)\Delta t. \quad (35)$$

The occupational probability change can also be related to the transition probabilities via:

$$\Delta\rho_{jj}(t) = -\rho_{jj}(t)\sum_k P_{j\to k}(t) + \sum_k \rho_{kk}(t)P_{j\leftarrow k}(t). \quad (36)$$

Thus $\Delta\rho_{jj}$, is dependent on both transition probabilities to and from states k, ($P_{j\to k}$, $P_{j\leftarrow k}$). Following Tully's fewest switches approach [9], transitions into state j are neglected. Equating (35) to (36) now yields:

$$\sum_k P_{j\to k}(t) = -\frac{\dot{\rho}_{jj}(t)\Delta t}{\rho_{jj}(t)}. \quad (37)$$

To determine the rate of change quantity, $\dot{\rho}_{jj}$, differentiate (33) with respect to time:

$$\dot{\rho}_{jj}(t) = \frac{\mathrm{d}}{\mathrm{d}t}\left[a_j^*(t)a_j(t)\right] \quad (38a)$$

$$\dot{\rho}_{jj}(t) = \frac{\mathrm{d}a_j^*(t)}{\mathrm{d}t}a_j(t) + a_j^*(t)\frac{\mathrm{d}a_j(t)}{\mathrm{d}t}. \quad (38b)$$

It can be shown that (38b) reduces to

$$\dot{\rho}_{jj}(t) = 2\,\mathrm{Re}\left(a_j^*(t)\frac{\mathrm{d}a_j(t)}{\mathrm{d}t}\right). \quad (39)$$

Substituting (8) into (39) yields:

$$\dot{\rho}_{jj}(t) = -2\,\mathrm{Re}\left(\sum_{k\neq j} a_j^*(t)a_k(t)\left\langle\boldsymbol{\phi}_j\left|\frac{\partial\boldsymbol{\phi}_k}{\partial t}\right\rangle \times \exp\left(-\frac{\mathrm{i}}{\hbar}\int_0^t E_k(\tau) - E_j(\tau)\,\mathrm{d}\tau\right)\right). \quad (40)$$

Now (33) and (40) can be substituted into (37)

$$\sum_k P_{j\to k} = \frac{2\Delta t}{a_j^*(t)a_j(t)}\,\mathrm{Re}\left(\sum_k a_j^*(t)a_k(t)d_{jk} \times \exp\left(-\frac{\mathrm{i}}{\hbar}\int_0^t E_k(\tau) - E_j(\tau)\,\mathrm{d}\tau\right)\right). \quad (41)$$

The transition probability from j to a specific state k can be extracted from (41):

$$P_{j\to k} = \frac{2\Delta t\,\mathrm{Re}\left(a_j^*(t)a_k(t)d_{jk}\exp\left[-(\mathrm{i}/\hbar)\int_0^t E_k(\tau) - E_j(\tau)\,\mathrm{d}\tau\right]\right)}{a_j^*(t)a_j(t)}. \quad (42)$$

Note d_{jk} is a real quantity provided the basis functions $\boldsymbol{\phi}_j$, $\boldsymbol{\phi}_k$ are real. Due to differences in the definition of the coupling term, d_{jk}, a sign difference is present between (42) and the derivation in [11].

4.2. *Velocity rescaling*

The sudden change in potential energy upon hopping from state j to k requires an equal change of kinetic energy for the system to conserve energy. This is accomplished by rescaling the nuclear velocities based on the nonadiabatic coupling terms, d_{jk} (12). The rationale, as proposed by Herman [17], is that the coupling terms drive the surface-hopping transitions. More specifically, the dot product of the coupling vector, $\boldsymbol{D}_{jk}$, and the velocity vector (or equivalently, the momentum vector $\boldsymbol{p}$) determine the value of the coupling terms. Thus only the component of the momentum parallel with the coupling vector influences the hopping probability. Conversely, upon hopping, only the component of the momentum parallel with the coupling vector would be expected to be affected by the kinetic energy readjustment. The hop is disallowed if it requires greater kinetic energy than available in the momentum parallel component.

For implementation, the momentum vector can be written in terms of parallel ($\boldsymbol{p}_\parallel$) and perpendicular ($\boldsymbol{p}_\perp$) components,

$$\boldsymbol{p} = \boldsymbol{p}_\parallel + \boldsymbol{p}_\perp, \tag{43}$$

where:

$$\boldsymbol{p}_\parallel = (\boldsymbol{p} \cdot \hat{\boldsymbol{D}}_{jk})\hat{\boldsymbol{D}}_{jk}, \tag{44}$$

$$\boldsymbol{p}_\perp = \boldsymbol{p} - \boldsymbol{p}_\parallel \tag{45}$$

and $\hat{\boldsymbol{D}}_{jk}$ as the unit vector $\boldsymbol{D}_{jk}/\|\boldsymbol{D}_{jk}\|$. The momentum gained or lost upon changing potential energy surfaces ($\Delta E = E_k - E_j$), reflects a new momentum value $p'_\parallel$,

$$\frac{(p'_\parallel)^2}{2m} = \frac{(p_\parallel)^2}{2m} - \Delta E \tag{46}$$

or

$$p'_\parallel = \left(p_\parallel^2 - 2m\Delta E\right)^{1/2}, \tag{47}$$

where the scalar momentum variables denote the norm of their corresponding momentum vectors. The new rescaled momentum, $\boldsymbol{p}'$, becomes:

$$\boldsymbol{p}' = \boldsymbol{p}_\perp + p'_\parallel \hat{p}_\parallel \tag{48}$$

and $\hat{\boldsymbol{p}}_\parallel$ as the unit vector $\boldsymbol{p}_\parallel/\|\boldsymbol{p}_\parallel\|$. Substituting (44) and (45) into (48) yields:

$$\boldsymbol{p}' = \boldsymbol{p} + p'_\parallel \hat{p}_\parallel - \left(\boldsymbol{p} \cdot \hat{D}_{jk}\right)\hat{D}_{jk}. \tag{49}$$

Descriptions of other methods used to rescale momentum are discussed in [11] and [18] and references therein.

5. Model system – avoided crossing

The following two-state system can illustrate the application of the mean-field and surface-hopping approaches. Based on an avoided crossing proposed by Tully [9], the energy and wave function evolution can be monitored over the course of a reaction event. Although the potential energy surfaces used in this example (Figure 2) are not intended to represent an existing chemical system, one could imagine analogous surfaces generated in a glancing collision trajectory. As a lighter, mobile atom is propelled toward a stationary heavier atom, the system approaches a potential energy (avoided) curve crossing, at which point nuclear dynamics exerts an influence on the molecular electronic wave function. The two state (adiabatic) potential energies (Figure 2) are determined through the diagonalisation of a 2×2 Hamiltonian:

$$\hat{\mathbf{H}}(\mathbf{r}) = \begin{bmatrix} V_{11}(r) & V_{12}(r) \\ V_{21}(r) & V_{22}(r) \end{bmatrix}, \tag{50}$$

where $V_{11}(r)$ and $V_{22}(r)$ are the diabatic potentials, and $V_{12}(r)$, $V_{21}(r)$ as the off-diagonal Gaussian

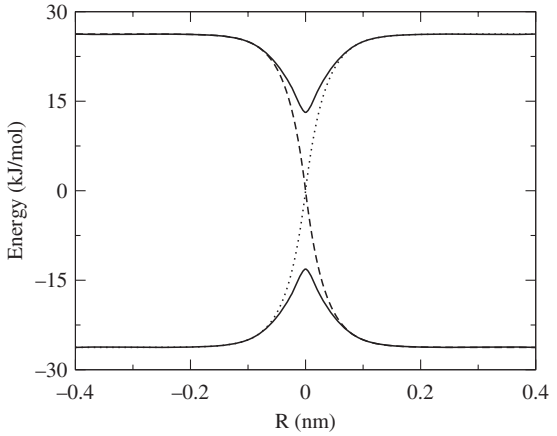

Figure 2. Diabatic potentials (V_{11} – dotted line, V_{22} – dashed line) defined by (51) and adiabatic potentials (E_0, E_1 – solid lines) by diagonalisation of (50).

mixing elements. The potential terms in (50) can take the following analytical forms:

$$\begin{aligned} V_{11}(r) &= A[1-\exp(-\beta r)], \quad r>0, \\ V_{11}(r) &= -A[1-\exp(\beta r)], \quad r<0, \\ V_{22}(r) &= -V_{11}(r), \\ V_{12}(r) &= V_{21} = C\exp(-Dr^2), \end{aligned} \tag{51}$$

where $A = 26\,\mathrm{kJ\,mol^{-1}}$, $\beta = 0.084\,\mathrm{nm}$ $C = 13\,\mathrm{kJ\,mol^{-1}}$, and $D = 0.0529\,\mathrm{nm}$. Molecular dynamics can be employed by integrating the nuclear equations of motion, e.g. with a velocity Verlet propagator [19]. The two approaches can be contrasted by monitoring the evolution of the electronic wavefunction.

Given the initial input parameters as specified in the caption, Figure 3 contrasts the spatial evolution the mean-field potential of the system as compared to adiabatic potential. Note that the asymptotic limit of the mean-field potential does not converge to either adiabatic surface, which is a limitation of the method. The values of the expansion coefficients (Figure 4), also correspondingly vary over the course of the trajectory but eventually converge to asymptotic values as the particles irrevocably separate. The asymptotic expansion coefficient values in this example can demonstrate the accuracy difference discussed in Sections 2.2 and 2.3 regarding calculations that employ analytical versus numerical phase propagation (Figure 5). The importance of employing the correctional term to the Hellmann–Feynman forces, (31), in the mean-field calculations is shown by the deviation of total energy conservation over the course of the reaction with respect to time (Figure 6).

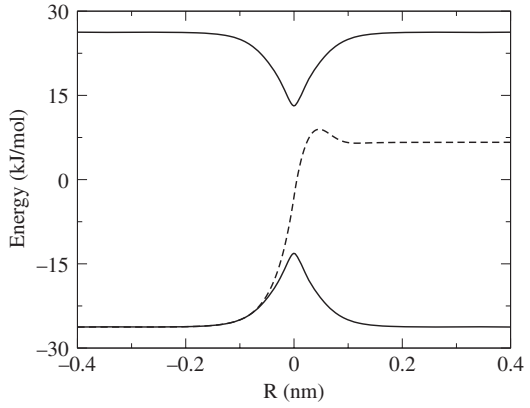

Figure 3. Potential energy (dashed line) versus coordinate of the trajectory on the potentials of (51) using the mean-field approach. Atom mass used was $1.82 \times 10^{-27}\,\mathrm{kg}$ (2000 au), at $t = 0$, $a_0 = 1$, $a_1 = 0$, $R = -0.432\,\mathrm{nm}$ (-8 bohr), and a momentum of $4.98 \times 10^{-14}\,\mathrm{kg\,nm\,s^{-1}}$ (25 au). The adiabatic potentials (solid lines) are plotted for reference.

Similarly, surface-hopping calculations can be run using the same input parameters as those specified for the mean-field calculations. The trajectory can be observed via a plot of the spatial evolution of potential energy surface (Figure 7). At the diabatic surface crossing region, $R = 0\,\mathrm{nm}$, it is apparent that the system temporarily 'hops' to the upper adiabatic surface, as predicted by the enhanced hopping probability in this spatial region (Figure 8). Note, that unlike the mean-field approach (Figures 3 and 4), the

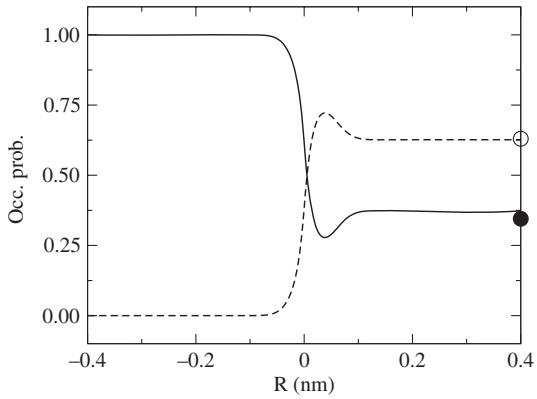

Figure 4. Space evolution of the expansion coefficients for the trajectory in Figure 3. At $t = 0$, $a_0^* a_0 = 1$ (solid line) and $a_1^* a_1 = 0$ (dashed line). Surface-hopping populations of two sets of 10,000 trajectories for simulations beginning on the corresponding lower (hollow circle) and upper (solid circle) states.

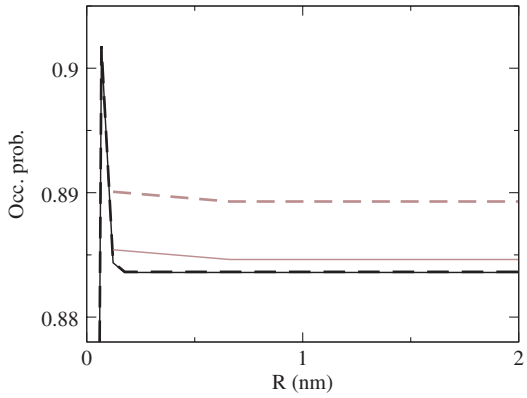

Figure 5. Influence of numerical and analytical electronic propagation as shown by the evolution of the $a_1^* a_1$ expansion coefficient of Figure 4. Trajectory convergence is observed from the numerical phase 0.10 fs step size (grey dashed line), analytical phase 0.10 fs step size (grey line), numerical phase 0.01 fs step size (black dashed line), to the analytical phase 0.01 fs step size (black line). The mean-field trajectories were calculated with an initial momentum of $9.96 \times 10^{-14}\,\mathrm{kg\,nm\,s^{-1}}$ (50 au) and identical remaining parameters as specified in Figure 4.

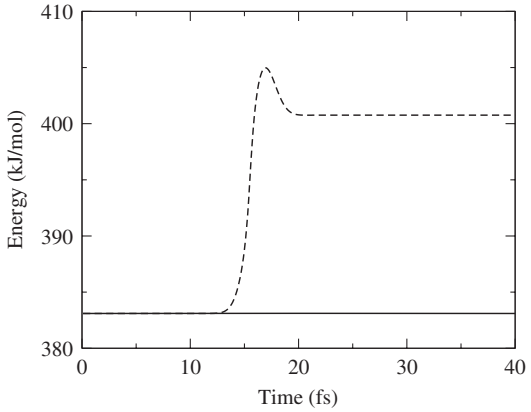

Figure 6. Total energy conservation for the trajectory in Figures 3 and 4 with (solid line) and without (dashed line) the addition of the second term (31) to the conventional Hellmann–Feynman forces.

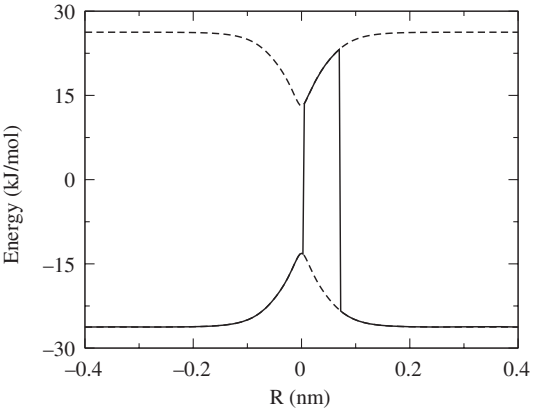

Figure 7. Potential energy of a typical surface-hopping trajectory (thick solid line) over the adiabatic potentials (dashed lines), with initial conditions specified in Figure 3.

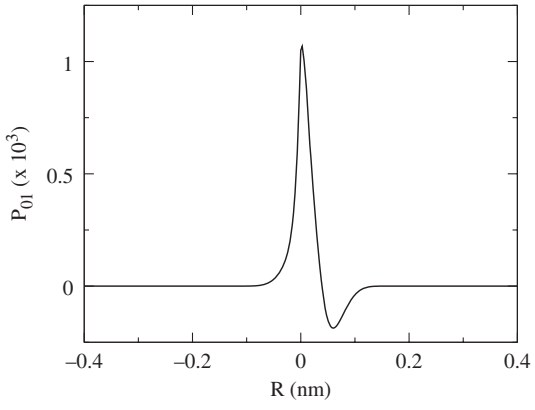

Figure 8. Hopping probability (42) for a non-hopping trajectory run on the ground surface with initial conditions specified in Figure 3.

asymptotic limit of the surface-hopping potential does properly converge to an adiabatic surface. A detailed discussion of the physical insight revealed by this and other simple prototypical examples are found in [9] and [11]. Although the mean-field and surface-hopping approaches can generate differing outcomes [12], we found good agreement of the resultant population ratios for both the Xe_3^+ photodissociation [15] and the present two-state example (Figure 4). For the latter, two sets of 10,000 surface-hopping trajectories were initialised with populations on the ground ($a_0^* a_0 = 1$) and excited ($a_0^* a_0 = 0$) states, yielded respective populations of 0.63 and 0.35, with the sum difference to unity attributed to sampling. For comparison, the mean-field trajectory yielded population values of 0.62 and 0.37 on the corresponding states.

6. Summary

The mean-field and surface-hopping methods are computationally economical, semi-classical approaches that include consideration of quantum effects on the dynamics of molecules. The present study has demonstrated the significance of two common, yet easily correctable, sources of accuracy loss regarding phase propagation and the necessity for inclusion of a Hellman–Feynman correctional term. Analytic derivation of the corresponding methods served to highlight the origin of energy conservation deviations and concepts were illustrated by simulations on two exemplar systems: the photodissociation of Xe_3^+ and a prototypical two-level, avoided crossing.

References

[1] H. Haberland, A. Hofmann and B.V. Issendorff, J. Chem. Phys. **103**, 3450 (1995).
[2] C. Frischkorn and M. Wolf, Chem. Rev. **106**, 4027 (2006).
[3] J.C. Tully, in *Modern Theoretical Chemistry: Dynamics of Molecular Collisions*, edited by W.H. Miller (Plenum Press, New York, 1996), pp. 217–267.
[4] G. Renger, in *Modern Theoretical Chemistry: Dynamics of Molecular Collisions*, edited by G. Renger (Royal Society of Chemistry, UK, 2008), pp. 5–38.
[5] M.R. Wasielewski, Chem. Rev. **92**, 435 (1992).
[6] H. Langer and N.L. Doltsinis, J. Chem. Phys. **118**, 5400 (2003).
[7] S. Hammes-Schiffer and J.C. Tully, J. Phys. Chem. **99**, 5793 (1995).
[8] M.P. Allen and D.J. Tildesley, *Computer Simulation of Liquids* (Oxford University Press, New York, 1987).
[9] J.C. Tully, J. Chem. Phys. **93**, 1061 (1990).
[10] P. Ehrenfest, Z. Phys. **45**, 455 (1927).

[11] D.F. Coker, in *Computer Simulation in Chemical Physics*, edited by M.P. Allen and D.J. Tildesley, April (Springer, CORISA, Alghero, Sardinia, 1993), pp. 315–378.
[12] J.C. Tully, in *Modern Methods for Multidimensional Dynamics Computations in Chemistry*, 1st ed., edited by D.L. Thompson (World Scientific, New Jersey, 1998), pp. 34–72.
[13] N.L. Doltsinis, in *Quantum Simulations of Complex Many-Body Systems: From Theory to Algorithms*, edited by J. Grotendorst, D. Marx and A. Muramatsu (John von Neumann Institute for Computing, Jülich, 2002), pp. 377–397.
[14] M.A. Porter, Rep. Prog. Phys. **64**, 1165 (2001).
[15] S.L. Fiedler, H. Kunttu and J. Eloranta, J. Chem. Phys. **128**, 164309 (2008).
[16] W.H. Press, S.A. Teukolsky, W.T. Vetterling and B.P. Flannery, *Numerical Recipes: the Art of Scientific Computing*, 3rd ed. (Cambridge University Press, New York, 2007).
[17] M.F. Herman, J. Chem. Phys. **84**, 262 (1984).
[18] A.I. Krylov, R.B. Gerber and R.D. Coalson, J. Chem. Phys. **105**, 4626 (1996).
[19] W.C. Swope, H.C. Andersen, P.H. Berens and K.R. Wilson, J. Chem. Phys. **76**, 637 (1982).

Appendix 1. Proof $\langle \boldsymbol{\phi}_j | (\partial \boldsymbol{\phi}_j / \partial t) \rangle = 0$ if $|\boldsymbol{\phi}_j\rangle$ is real

$$\langle \boldsymbol{\phi}_j | \boldsymbol{\phi}_j \rangle = 1, \tag{52}$$

$$\frac{\partial}{\partial t} \langle \boldsymbol{\phi}_j | \boldsymbol{\phi}_j \rangle = \frac{\mathrm{d}}{\mathrm{d}t}(1), \tag{53}$$

$$\left\langle \frac{\partial \boldsymbol{\phi}_j}{\partial t} \middle| \boldsymbol{\phi}_j \right\rangle + \left\langle \boldsymbol{\phi}_j \middle| \frac{\partial \boldsymbol{\phi}_j}{\partial t} \right\rangle = 0. \tag{54}$$

Take the complex conjugate twice of the second term in (54),

$$\left\langle \boldsymbol{\phi}_j \middle| \frac{\partial \boldsymbol{\phi}_j}{\partial t} \right\rangle = \left\langle \frac{\partial \boldsymbol{\phi}_j}{\partial t} \middle| \boldsymbol{\phi}_j \right\rangle^*. \tag{55}$$

Substituting (55) into (54) yields,

$$\left\langle \frac{\partial \boldsymbol{\phi}_j}{\partial t} \middle| \boldsymbol{\phi}_j \right\rangle + \left\langle \frac{\partial \boldsymbol{\phi}_j}{\partial t} \middle| \boldsymbol{\phi}_j \right\rangle^* = 0. \tag{56}$$

The proof can be completed here since all quantities in (56) are real,

$$\left\langle \frac{\partial \boldsymbol{\phi}_j}{\partial t} \middle| \boldsymbol{\phi}_j \right\rangle = 0. \tag{57}$$

If $\boldsymbol{\phi}_j$ contains a complex component, the $\langle \boldsymbol{\phi}_j | (\partial \boldsymbol{\phi}_j / \partial t) \rangle$ term in (8) and (11) should be addressed [18].